2010

Dynamics of fibrillar precursors of shishes as a function of stress

Luigi Balzano
Eindhoven University of Technology

Dario Cavallo
University of Genova

Tim B. van Erp
Eindhoven University of Technology

Zhe Ma
Eindhoven University of Technology

Jan-Willem Housmans
Eindhoven University of Technology

See next page for additional authors

IOP Conf. Series: Materials Science and Engineering **14** (2010) 012005 doi:10.1088/1757-899X/14/1/012005

Dynamics of fibrillar precursors of shishes as a function of stress

Luigi Balzano[1,4], Dario Cavallo[3], Tim B. van Erp[1], Zhe Ma[1,4], Jan-Willem Housmans[1], Lucia Fernandez-Ballester[2], Gerrit W.M. Peters[1,4]

[1]Department of Mechanical Engineering

Eindhoven University of Technology

P.O. Box 513, 5600 MB Eindhoven, The Netherlands

[2]DUBBLE CRG/ESRF, Netherlands Organization for Scientific Research (NWO)

c/o ESRF BP 220 , F-38043, Grenoble Cedex, France

[3]Department of Chemistry and Industrial Chemistry

University of Genova, Via Dodecaneso 31, 16146 Genova, Italy

[4]Dutch Polymer Institute (DPI),

P.O. Box 902, 5600 AX Eindhoven, The Netherlands

Email: G.W.M.Peters@tue.nl

Abstract. Shishes are fibrillar crystallites that can be created by deforming a polymer melt. The formation of shishes takes place when flow is strong enough to stretch molecules. In the early stages, bundles of stretched molecules with pre-crystalline order form metastable precursors whose stability depends on their size and, hence, on the stress level. We find that for a specific isotactic polypropylene, close to the nominal melting point, a stress larger than 0.10 MPa leads to stable fibrillar precursors that are partially crystalline immediately after flow. On the other hand, below 0.10 MPa, the aspect ratio of precursors tends to unity and the lack of crystallinity makes these structures prone to dissolution.

1. Introduction

Shishes are fibrillar crystallites formed by macromolecules, extended under the influence of stress, both in melts as well as in solutions [1-3]. The interest in these structures arises from the large influence that they have on the properties of materials. Shishes promote anisotropic and well packed crystalline morphologies that enhance stiffness, wear and permeability. Elucidating the molecular mechanism for their formation offers the opportunity for designing molecules and processes to tailor material properties.

During flow-induced crystallization (FIC), in the early stages of shish formation, the stretch of the physical network of entangled molecules gives rise to fibrillar precursors of the emerging structures [4-9]. These flow induced precursors (FIPs) are bundles of stretched molecules with pre-crystalline order and density higher than the melt [10]. The dynamics of FIPs is suggested to be related to external conditions and their size [11-13], however little information is available. In this Article, we analyze quantitatively the effect of stress on the dynamics of FIPs using an isotactic polypropylene (iPP) as a model system. Experiments are carried out with time resolved X-ray scattering in combination with slit flow, a powerful tool for flow induced crystallization studies [14-16].

2. Material

The material investigated is an isotactic polypropylene homopolymer (HD120M0, supplied by Borealis GmbH) with molecular weight M_w=365 kg/mol, molecular weight distribution MWD=5.4 (i.e. M_n=68 kg/mol) and tacticity 97.5 %mmmm (from FTIR). The nominal melting point (DSC at 10 °C/min) is 163 °C. From rheometry (dynamic measurements), the disengagement time, related to the high molecular weight tail is determined to be τ_D=25 s and the corresponding stretch relaxation time is τ_s=0.12 s at 165 °C [17].

3. Methods

Small and wide angle X-ray scattering (SAXS and WAXS) were performed at the beamline BM26B [18] of the European Synchrotron Radiation Facility (Grenoble, France) with a wavelength λ=1.0 Å. For SAXS, a gas filled detector with 512 x 512 pixels of 260 μm x 260 μm was used to collect images at 6.4 m from the sample with an exposure time of 3 s. While, for WAXS, a CCD detector (Photonic Science, UK) with 2000 x 1336 pixels of 44 μm x 44 μm was placed at 0.18 m and an exposure time of 5 s was used. SAXS and WAXS images were processed with the software Fit2D.

Crystallization was investigated using a short term shear [15, 19] protocol in a custom-built slit flow cell mounted on a Multi-Pass Rheometer (MPR). The slit has cross section of 1.5 mm x 6 mm and length of 120 mm. The specimen is sheared by moving two pistons (diameter 12 mm), placed in reservoirs at both ends of the slit, simultaneously upwards or downwards. The maximum displacement of the pistons is designed in such a way that the material initially in the reservoir (going through a contraction) does not arrive in the observation window. For all experiments discussed in this here, the displacement of the pistons is 3 mm. To obtain an optimal filling of the slit and rule out wall slippage, prior to the actual experiment, the specimen is pressurized up to 100 bar by bringing the two pistons towarde each other. When the pistons move, the shear rate $\dot{\gamma}$ increases from the centerline (where $\dot{\gamma} = 0$) until the wall (where $\dot{\gamma} = \dot{\gamma}_w$). The wall shear rate $\dot{\gamma}_w$ is determined by the speed of the pistons and geometrical parameters of the slit. More details are provided elsewhere [17]. When the rheology of the material is known, the stress profile in the specimen, which increases linearly from the centerline ($\sigma = 0$), to the wall ($\sigma = \sigma_w$), can be calculated as well [20].

4. Results and Discussion

Shearing a polymer melt can lead to the formation of a large number of flow induced precursors of crystallization (FIPs) also at temperatures close to the nominal melting point [4, 21, 22]. Depending on the conditions, FIPs eventually lead to fibrillar (needle-like) crystals with varying aspect ratio [23]. Here, we investigate the effect of the level of the shear stress on the average size and stability of FIPs after cessation of flow in isotactic polypropylene (iPP). The focus is on isothermal short term shear at 165 °C, close to the nominal melting point (163 °C). The flow conditions, given in Table 1, are chosen to ensure a large Deborah stretch number ($De_s = \dot{\gamma} \cdot \tau_s$) and, therefore, orientation and stretch of molecular segments [24]. At every wall stress σ_w , the shear time t_s is adjusted to keep the overall displacement of the pistons always at 3 mm.

Table 1. Experimental conditions at 165 °C. Pistons displacement = 3 mm (total shear $\gamma_{max} = 220$).

σ_w [MPa]	t_s [s]	Wall shear rate $\dot{\gamma}_{wall}$ [s^{-1}]	Wall Deborah stretch $De^s_{wall} = \tau_s \dot{\gamma}_{wall}$
0.19	0.182	1180	135
0.14	0.375	590	68
0.12	0.500	442	51
0.10	0.750	295	34
0.08	1.500	147	17

The formation of (a large amount of) fibrillar FIPs, aligned in the flow direction, is accompanied by the onset of an equatorial streak of intensity in the SAXS [4, 25, 26]. The images shown on the right side of Figure 1 indicate that the formation of these fibrillar FIPs occurs at stresses larger than 0.12 MPa.

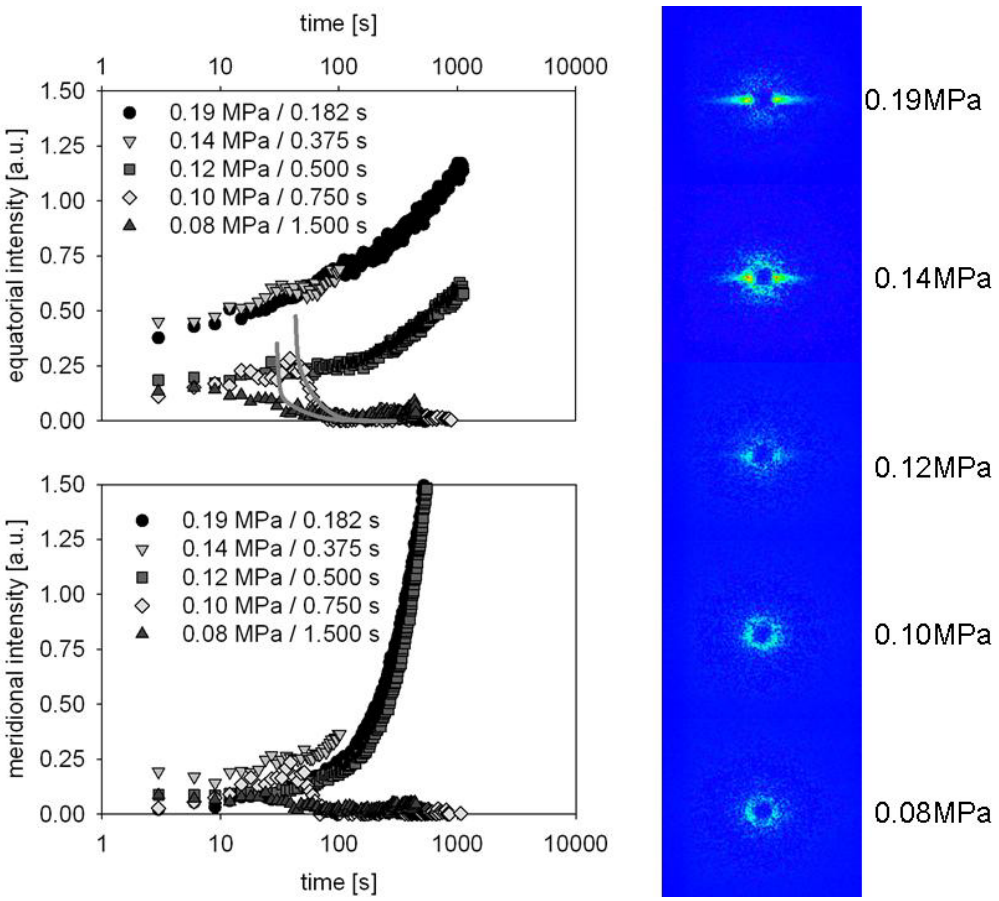

Figure 1: left) Meridional and equatorial intensities from SAXS at 165 °C after application of shear. The lines in the plot of the equatorial intensity represent the Doi-Edwards memory function. right) SAXS patterns after cessation of flow for different flow conditions.

A more thorough analysis of the images reveals that precursors are formed at lower stress too, but with different properties. To highlight these differences, the experiments of Figure 1 are grouped in two categories and discussed hereafter.

Stress larger than 0.12 MPa. - For $\sigma_w \geq 0.12$ MPa, stable fibrillar FIPs are formed. Despite the high temperature, these FIPs rapidly crystallize, perhaps already during the shear pulse. In fact, weak diffraction peaks are already observed in the first WAXS images after flow (see Fig. 2). The ratio between crystalline and amorphous scattering yields a crystallinity $X_{t=0}$ approximated with 0.2 % for 0.19 MPa, 0.1 % for 0.14 MPa and not quantifiable for 0.12 MPa. Since FIPs are aligned oblong bundles of stretched molecules, the most efficient method to visualize the diffraction is sampling the intensity along the 2θ direction following the azimuthal positions of the maxima, after subtraction of the amorphous halo (melt frame), as illustrated in Figure 2a.

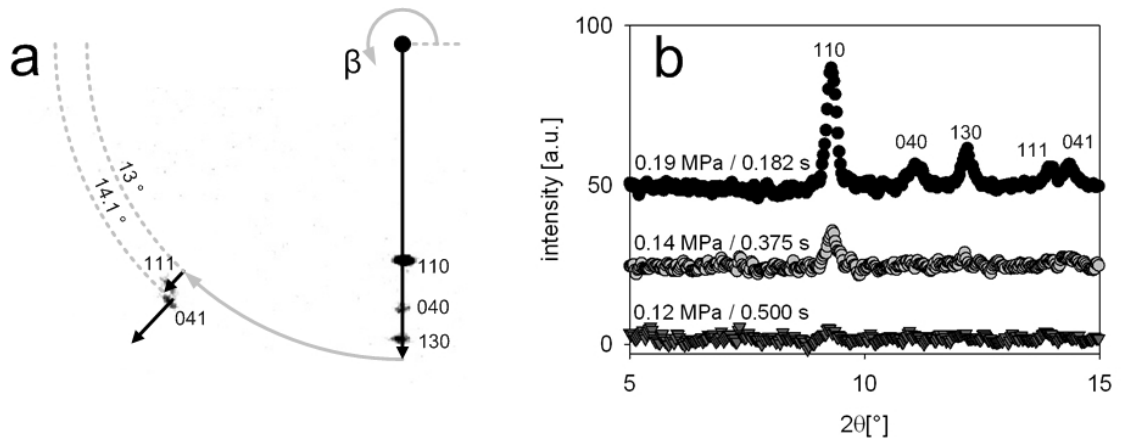

Figure 2: a) 2θ path for visualizing the structure of fibrils. Azimuthal switches take place at 2θ=13 ° (β from -90 to -132 °) and at 2θ=14.1 ° (β from -132 to -130 °); b) Intensity scans on the first image acquired after flow.

The result, shown in Figure 2b, indicates that the iPP fibrils are already partially crystalline with a well developed α crystal structure for a stress of 0.19 MPa. Intensities are taken from the first image acquired after flow. At lower stress, diffraction peaks are less intense (but still clear for a stress of 0.14 MPa suggesting a lower crystallinity and possibly a less perfect structure. WAXS shows that, with time, FIPs crystallize and the intensity of the SAXS equatorial streak increases as shown in the top-left panel of Figure 1.

The SAXS images provide the average dimensions of the fibrils for varying σ_w. The Guinier's plot of the cross section [27], reveals that the average fibril diameter is D=26 nm. Length and orientation are determined from the equatorial streak using the deconvolution method proposed by Ruland [28-30]. The azimuthal width of the streak contains contributions from length and orientation of the fibrils (besides a negligible contribution from the beam size). With the assumption that both distributions have a Lorentzian profile, the individual contributions are separated using the Warren-Averbach theorem [31]:

$$B_{obs} = \frac{1}{L \cdot s} + B_{or} \qquad (1.1)$$

where B_{obs} is the observed azimuthal width, L and B_{or} are, respectively, the average fibril length and orientation and $s = 2/\lambda \cdot \sin\theta$ is the modulus of the scattering vector (with 2θ being the scattering angle). To reduce the influence of noise, L and B_{or} are evaluated from an 'artificial' image obtained by summing up the first 20 images of the experiment, i.e. with an effective exposure time of 60 s and negligible noise. One of the corresponding Ruland's plot is shown in Figure 3.

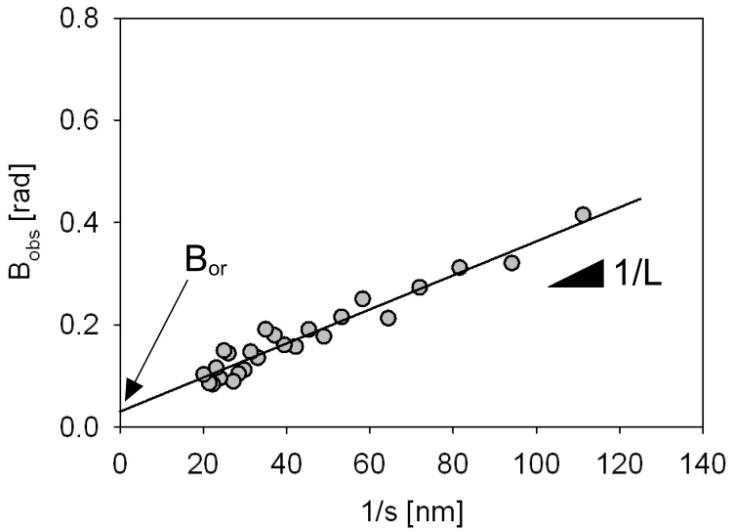

Figure 3: Ruland's plot used to determine the length of fibrils from the width of the equatorial streak in SAXS. The line represents the fit with Eq. (1.1).

The results for σ_w>0.12 MPa, given in Table 2, show that, despite the lower shear time, higher stresses generate longer fibrils. With these data at hand, the aspect ratio (L/D) of stable fibrils is 11.3 for 0.19 MPa and 9.3 for 0.14 MPa.

Table 2 Details on size and initial crystallinity of fibrils.

	0.19 MPa / 0.182 s	0.14 MPa / 0.375 s
L [nm]	293	242
B_{or} [rad]	0.028	0.024
L/D	11.3	9.3
$X_{t=0}$ [%]	0.2	0.1

Flow deforms molecules transforming coils into fibrils. The maximum deformation rate can be estimated as $\dot{L}_{flow}^{max} = \dot{\gamma} \cdot 2R_g$, where R_g=4.1 nm [1] is the radius of gyration. On the other hand, the minimum rate of transformation can be estimated from the experiments with the longitudinal growth rate of the fibrils expressed as $\dot{L}_{flow}^{min} = L / t_s$, i.e. as the ratio between the length of the fibrils and the shear time. The values obtained for $\dot{L}_{flow}^{min}$ are comparable with the highest growth rate in quiescent conditions [32] and are just about 1/10 of $\dot{L}_{flow}^{max}$ (see Table 3).

Table 3 Maximum and minimum longitudinal growth rate of the fibrils.

	0.19 MPa / 0.182 s	0.14 MPa / 0.375 s
$\dot{L}_{flow}^{min}$ [nm/s]	$1.6 \cdot 10^3$	$0.6 \cdot 10^3$
$\dot{L}_{flow}^{max}$ [nm/s]	$9.7 \cdot 10^3$	$4.8 \cdot 10^3$

[1] $R_g = \sqrt{N_{mon}/6} \cdot L_{mon}$, where the number of monomers $N_{mon} = M_n / 42$ and the length of a monomer $L_{mon} = 2 \cdot 1.54 \cdot Sin(109.5/2)$ Å.

Stress smaller than 0.12 MPa. - When σ_w<0.12 MPa, no diffraction peak is observed in WAXS immediately after shear and FIPs are not stable. They have a limited lifetime and dissolve back in to the melt, decreasing the SAXS equatorial intensity. The poor stability of FIPs is attributed to their short length. With the ends of the fibrils too close to each other, these precursors have a high concentration of defects that triggers the dissolution. The short length of FIPs is confirmed by scattered intensity that, though higher than the melt, does not vary in the azimuth, also at low scattering angles. This indicates that the aspect ratio of FIPs tends to unity, i.e. their length approaches their diameter that is 26 nm or lower. Despite the dissolution starts at different times (33 s for 0.08 and 45 s for 0.10 MPa), the time constant of the process is the same (i.e. ~21 s) and matches the disengagement time of the high molecular weight tail τ_D. This suggests that dissolution of small FIPs is determined by reptation of the longest molecules of the melt. This hypothesis is strengthened by the good description that the Doi-Edwards memory function [4, 33]

$$\mu(t) = \frac{8}{\pi^2} \cdot \sum_{p\,odd} \frac{1}{p^2} \exp\left(-p^2 \frac{t - t_0}{\tau_D} \right) \tag{1.2}$$

with τ_D=21 s represents the drop of the equatorial intensity rather well (lines in the equatorial intensity plot of Figure 1). Such a scenario is consistent with short precursors based on a scaffold of the longest molecules. These molecules extended by the flow diffuse out of FIPs with reptative motions.

5. Conclusions

In the early stages of the formation of shishes, metastable fibrillar bundles of stretched molecules (flow induced precursors of crystallization, FIPs) exhibit a size- and, therefore, stress-dependent dynamics. In iPP, at high stress, FIPs can reach a length close to 300 nm and are stabilized by crystallization immediately after flow. At low stress, FIPs are much shorter and their aspect ratio tends to unity. The lack of crystallinity immediately after flow makes these structures prone to dissolution. Interestingly, the dissolution time-scale matches the relaxation time of the longest molecules of the melt suggesting that the scaffold of small FIPs is based on high molecular weight molecules and the dissolution mechanism involves their reptation.

This work is part of the Research Programme of the Dutch Polymer Institute (DPI), P.O. Box 902, 5600 AX Eindhoven, The Netherlands, projectnrs. #634 and #714.

6. References

[1] F. L. Binsbergen, Nature **211**, 516 (1966).
[2] J. Pennings, and A. M. Kiel Kolloid ZZ Polym **205**, 160 (1965).
[3] Z. Bashir, J. A. Odell, and A. Keller, Journal of Materials Science **19**, 3713 (1984).
[4] L. Balzano *et al.*, Physical Review Letters **100**, 048302 (2008).
[5] L. Balzano, S. Rastogi, and G. W. M. Peters, Macromolecules **42**, 2088 (2009).
[6] G. Kumaraswamy *et al.*, Macromolecules **35**, 1762 (2002).
[7] G. Matsuba *et al.*, Macromolecules **40**, 7270 (2007).
[8] L. Fernandez-Ballester *et al.*, Journal of Synchrotron Radiation **15**, 185 (2008).
[9] F. Custodio *et al.*, Macromol. Theory Simul. **18**, 469 (2009).
[10] R. H. Somani *et al.*, Macromolecules **38**, 1244 (2005).
[11] F. Azzurri, and G. C. Alfonso, Macromolecules **38**, 1723 (2005).
[12] F. Azzurri, and G. C. Alfonso, Macromolecules **41**, 1377 (2008).
[13] G. H. Eder, H. Janeschitz-Kriegl, and G. Krobath, Prog. Colloid Polym. Sci. **80**, 1 (1989).

[14] M. Seki *et al.*, Macromolecules **35**, 2583 (2002).
[15] P. Jerschow, and H. Janeschitz-Kriegl, International Polymer Processing **12**, 72 (1997).
[16] H. Janeschitz-Kriegl, E. Ratajski, and M. Stadlbauer, Rheol. Acta **42**, 355 (2003).
[17] J. W. Housmans *et al.*, International Polymer Processing **XXIV**, 185 (2009).
[18] W. Bras *et al.*, Journal of Applied Crystallography **36**, 791 (2003).
[19] P. Jerschow, and H. Janeschitz-Kriegl, Rheol. Acta **35**, 127 (1996).
[20] C. Macosko, *Rheology : principles, measurements, and applications* (VCH, Weinheim, 1994).
[21] R. H. Somani, I. Sics, and B. S. Hsiao, Journal of Polymer Science Part B: Polymer Physics **44**, 3553 (2006).
[22] N. Kukalyekar *et al.*, Macromolecular Reaction Engineering **3**, 448 (2009).
[23] R. M. Gohil, and J. Petermann, Journal of Materials Science **18**, 1719 (1983).
[24] J. van Meerveld, G. W. M. Peters, and M. Hutters, Rheol Acta **44**, 119 (2004).
[25] N. Stribeck, Journal of Polymer Science Part B: Polymer Physics **37**, 975 (1999).
[26] R. H. Somani *et al.*, Polymer **46**, 8587 (2005).
[27] A. Guinier, and G. Fournet, *Small-angle scattering of X-rays* (Chapman & Hall, London, 1955).
[28] W. Ruland, Journal of Polymer Science: Part C **28**, 143 (1969).
[29] N. Stribeck, *X-ray scattering of soft matter* (Springer-Verlag, Berlin, 2007).
[30] B. X. Fu *et al.*, Polymers **42**, 599 (2001).
[31] B. E. Warren, *X-ray Diffraction* (Dover, New York, 1990).
[32] G. H. Eder, and H. Janeschitz-Kriegl, in *Processing of Polymers. Structure Development during Processing*, edited by H. E. H. Meijer (Wiley–VCH, Weinheim, 1997), pp. 269.
[33] M. Doi, and S. F. Edwards, *The theory of polymer dynamics* (Clarendon Press, Oxford, 1986).